



Colloidal Synthesis of NbS₂ Nanosheets: From Large-Area Ultrathin Nanosheets to Hierarchical Structures

Wenhui Li¹, Xijun Wei¹, Hongmei Dong¹, Yingqing Ou¹, Shenghuan Xiao¹, Yang Yang¹, Peng Xiao^{2*} and Yunhuai Zhang^{1*}

¹ College of Chemistry and Chemical Engineering, Chongqing University, Chongqing, China, ² College of Physics, Chongqing University, Chongqing, China

OPEN ACCESS

Edited by:

Junlei Qi,
Harbin Institute of Technology, China

Reviewed by:

Kaibing Xu,
Donghua University, China
Xudong Liu,
China Academy of Engineering
Physics, China

*Correspondence:

Peng Xiao
xiaopeng@cqu.edu.cn
Yunhuai Zhang
xp2031@163.com

Specialty section:

This article was submitted to
Nanoscience,
a section of the journal
Frontiers in Chemistry

Received: 08 February 2020

Accepted: 28 February 2020

Published: 07 April 2020

Citation:

Li W, Wei X, Dong H, Ou Y, Xiao S,
Yang Y, Xiao P and Zhang Y (2020)
Colloidal Synthesis of NbS₂
Nanosheets: From Large-Area
Ultrathin Nanosheets to Hierarchical
Structures. *Front. Chem.* 8:189.
doi: 10.3389/fchem.2020.00189

Layered NbS₂, a member of group-V transition metal dichalcogenides, was synthesized via a colloidal synthesis method and employed as a negative material for a supercapacitor. The morphologies of NbS₂ can be tuned from ultrathin nanosheets to hierarchical structures through dynamics controls based on growth mechanisms. Electrochemical energy storage measurements present that the ultrathin NbS₂ electrode exhibits the highest rate capability due to having the largest electrochemical surface area and its efficient ion diffusion. Meanwhile, the hierarchical NbS₂ shows the highest specific capacitance at low current densities for small charge transfer resistance, displays 221.4 F g⁻¹ at 1 A g⁻¹ and 117.1 F g⁻¹ at 10 A g⁻¹, and cycling stability with 78.9% of the initial specific capacitance after 10,000 cycles. The aggregate or stacking of nanosheets can be suppressed effectively by constructing hierarchical structure NbS₂ nanosheets.

Keywords: colloidal synthesis, morphology regulation, niobium disulfide nanosheets, supercapacitor, transition metal dichalcogenides

INTRODUCTION

Layered transition-metal dichalcogenides (TMDs), which have a X-M-X sandwich structure (generalized formula: MX₂, M = transition metal element; X = S, Se, or Te) in each layer, have attracted extensive attention due to their great potential for applications in energy storage (Chhowalla et al., 2013; Muller et al., 2015; Lin et al., 2019), catalysis (Yan et al., 2014; Yang et al., 2019), electronics (Wang et al., 2012; Lin et al., 2018), photonics (Mak and Shan, 2016; Linhart et al., 2019) etc. Recently, significant progress has been made on TMDs materials for energy storage applications (Han et al., 2018; Yun et al., 2020). However, a crucial issue regarding practical use is the aggregation or restacking of the individual layers with high surface energy by interlayer van der Waals forces (Chhowalla et al., 2013), which can cause low coulombic efficiency and capacity degradation irreversibly (Mei et al., 2018).

To solve the aggregation or restacking problem, some strategies to optimize the structure of TMDs materials have been proposed in previous studies. One strategy is to construct TMDs/conductor composites, e.g., grapheme (Li et al., 2011; Yang et al., 2017), carbon nanotubes (Wang et al., 2019), carbon nanofibers (Cha et al., 2017), organic polymers (Cho et al., 2019), etc., which can suppress the aggregation of layered TMDs effectively. Another important strategy is to adjust the structure parameters in the synthesis process. For instance, to tune the size and thickness

of nanosheets (Yin and Alivisatos, 2005; Yoo et al., 2014; Mansouri and Semagina, 2018), increase the layer-to-layer spacing (Jang et al., 2011), or construct hierarchical architectures (Sun et al., 2014; Cong et al., 2017; Zhang J. et al., 2017).

Among layered TMDs, group-V 2H-NbS₂ has an intrinsic metallic character owing to the half-filled $4d_{z^2}$ orbital (Kuc et al., 2011). The good electric conductivity and preferable flexibility of 2H-NbS₂ are practical for applications in energy storage (Han et al., 2018). However, the control of the morphologies, growth mechanism, and the structure-property relationship still need to be further explored. Therefore, this paper regulated the reaction dynamics of the colloidal synthesis process of 2H-NbS₂ by adjusting growth temperature and the amount of carbon disulfide, obtaining different morphologies of NbS₂, such as ultrathin nanosheets, self-assembled hierarchical structures, and layer stacked nanosheets. Furthermore, the growth mechanism was illustrated, and the effect of morphologies on supercapacitor performance was investigated.

EXPERIMENTAL SECTION

Chemicals

Niobium (V) chloride (NbCl₅, 99.9%), carbon disulfide (CS₂, 99.9%), and oleylamine (80–90%) were purchased from Aladdin Ltd. Potassium chloride (KCl), Hexane, n-butanol, and absolute ethanol were of analytical grade and all obtained from Chuan Dong Ltd.

Synthesis of NbS₂ Nanosheets

A slight modified colloidal synthesis method is used to synthesize NbS₂ nanosheets (Jeong et al., 2012). First, NbCl₅ (1 mmol, 0.27 g) and oleylamine (24.3 mmol, 8.0 mL) was added to a 100 mL three-neck flask under Ar atmosphere. Next, the mixture was treated under ultrasound until completely dissolved of NbCl₅ to form yellow transparent liquid. Then the mixture was heated to 120°C for 30 min under an Ar flow to remove water and oxygen. After the solution was heated to 300°C, CS₂ (30 mmol, 1.8 mL) was injected dropwise into the hot solution at a speed of ~1 mL/min. The reaction proceeded at 300°C for 2 h before being stopped by removal from the heating mantle. The NbS₂ nanosheets were precipitated by addition of excess butanol, and washed by mixed solution of hexane and absolute ethanol (1:1), and DI water for several times. Finally, the brownish black NbS₂ powder was obtained by a freeze-drying method. To regulate the morphologies of NbS₂, the reaction temperature was set at 280, 300, and 320°C, and the CS₂ amount was adjusted as 10, 30, and 60 mmol, respectively, and other experiment parameters remained unchanged.

Material Characterization

Scanning electron microscopy (SEM) images were taken on a field-emission scanning electron microscope (FESEM, FEI Nova 400 Nano-SEM). A high-resolution transmission electron microscope (HRTEM, ThermoFisher Scientific, Talos F200s) was performed to analyze the structures and elemental mapping. X-ray diffraction (XRD) patterns of the as-synthesized NbS₂ were recorded on a diffractometer with Cu K α radiation

(Spectris Pte. Ltd, PANalytical X' Pert Powder). Chemical states of the containing elements were analyzed by X-ray photoelectron spectroscopy (XPS, Thermo Scientific ESCALAB 250Xi, K-alpha). Fourier transform infrared (FTIR) spectrometer (ThermoFisher Scientific, Nicolet iS50) was used to analyze the composition of the samples.

Electrochemical Measurement

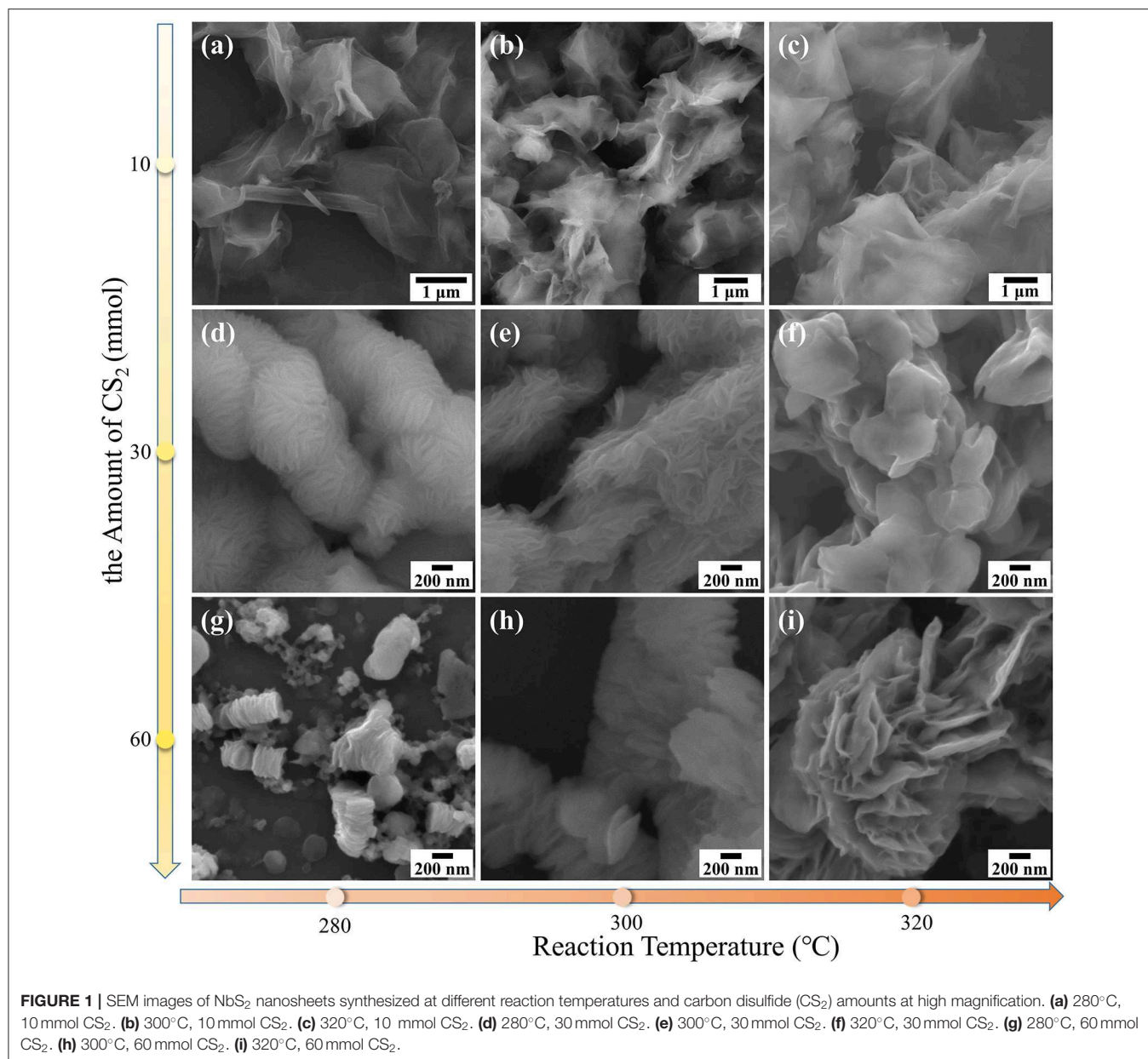
The electrochemical performance of NbS₂ nanosheets for the supercapacitor was measured by using a three-electrode cell system at room temperature. Specifically, the active material (70 wt%), conductive carbon black (20 wt%), and polyvinylidene fluoride binder (10 wt%) were mixed and turned into slurry uniformly, using absolute ethanol. Then the slurry was coated onto the pre-cleaned nickel foam with mass loading of active material ~1.5 mg cm⁻². After being dried in a vacuum oven at 60 °C overnight, the nickel foam coated with active material and another pre-cleaned nickel foam were overlapped and pressed at 10 MPa and used as a working electrode. A platinum foil and an Ag/AgCl (saturated KCl) electrode were used as the counter and reference electrode, respectively. The electrochemical performance was tested in 1 M KCl electrolyte solutions. Cyclic voltammetry (CV), galvanostatic charge-discharge (GCD) curves and electrochemical impedance spectroscopy (EIS) were tested using an electrochemical workstation (CHI660E, CH Instruments). Cycling stability tests were carried out on an electrochemical instrument (LAND).

RESULTS AND DISCUSSION

Physical Characterization of NbS₂ Nanosheets

The morphologies of NbS₂ nanosheets can be tuned by adjusting the reaction conditions. The lateral size, thickness, and assembly mode of NbS₂ nanosheets varied with the reaction temperature and the amount of carbon disulfide (CS₂), as observed by SEM images [Figure 1 (high magnification), Figure S1 (low magnification)]. The materials exhibited large lateral size and ultrathin nanosheets when using 10 mmol CS₂ as the sulfur source at a reaction temperature of 280, 300, and 320°C (Figures 1a–c, Figures S1a–c). The lateral size of the nanosheets was ~2 μ m at 280°C, ~3 μ m at 300°C, and ~4 μ m at 320°C, and showed an increasing trend with reaction temperature. Scrolled structures could be observed at the edges of the ultrathin films. The nanosheets formed unavoidable wrinkles as a self-folding phenomenon to balance adhesion energy and bending strain energy, which can cause the intrinsic lattice structures to distort (Chen et al., 2019).

With the increase of the amount of CS₂, the NbS₂ nanosheets tended to assemble to form hierarchical or stacked structures, including both vertically assembled (face-to-face) and laterally gathered (edge-to-edge) ways (Zhang X. et al., 2017), and the lateral size showed a decreasing trend while the thickness increased. Under the reaction condition of 300°C and 30 mmol CS₂, the materials grew to hierarchical structures, composed of nanosheets with lateral sizes of ~700 nm (hierarchical NbS₂, Figure 1e, Figure S1e). When the amount of CS₂ was increased



to 60 mmol at 300 °C, the NbS₂ structures was assembled by layer-stacked nanodisks, which lateral size reduced to ~500 nm (stacked NbS₂, **Figure 1h**, **Figure S1h**). At 280 °C and 60 mmol CS₂ conditions, the nanodisks with diameters of ~300 nm were mainly vertically assembled, like granum that stack thylakoids (**Figure 1g**, **Figure S1g**). At 320°C and 60 mmol CS₂ conditions, the nanosheets with diameters of ~1 μm formed flower-like structures (**Figure 1i**, **Figure S1i**). Overall, the lateral size and thickness of NbS₂ nanosheets increased with the temperature. With the increasing amount of CS₂, the lateral size decreased and the thickness increased.

To simplify the study, the ultrathin, hierarchical, and stacked NbS₂ nanosheets in the following test results of this essay refer to the samples synthesized using 10, 30, and 60 mmol CS₂ at 300°C, corresponding to **Figures 1b,e,h** respectively.

The TEM images of the NbS₂ nanosheets are shown in **Figure 2**. The lateral size of the ultrathin NbS₂ nanosheets was about 3 μm (**Figure 2a**). The lattice fringes of the ultrathin nanosheet presented in HRTEM images indicate the as-prepared NbS₂ was in 2H phase (**Figure 2b**). The interplanar spacings of 2.8 and 1.7 Å corresponded to the (100) and (110) plane of 2H-NbS₂ (Jeong et al., 2012). The diffraction rings in the selected area electron diffraction (SAED) pattern illustrated a polycrystalline nature, which can be assigned to (100), (110), and (200) planes, respectively (**Figure 2c**). The element mapping of the scanning transmission electron microscope-energy dispersive spectroscope (STEM-EDS) presented the uniform distributions of Nb and S in the nanosheets (**Figures 2d–f**). **Figures 2g–i** show the edges of ultrathin, hierarchical, and stacked nanosheets, corresponding to **Figures 1b,e,h**, respectively. The enlarged

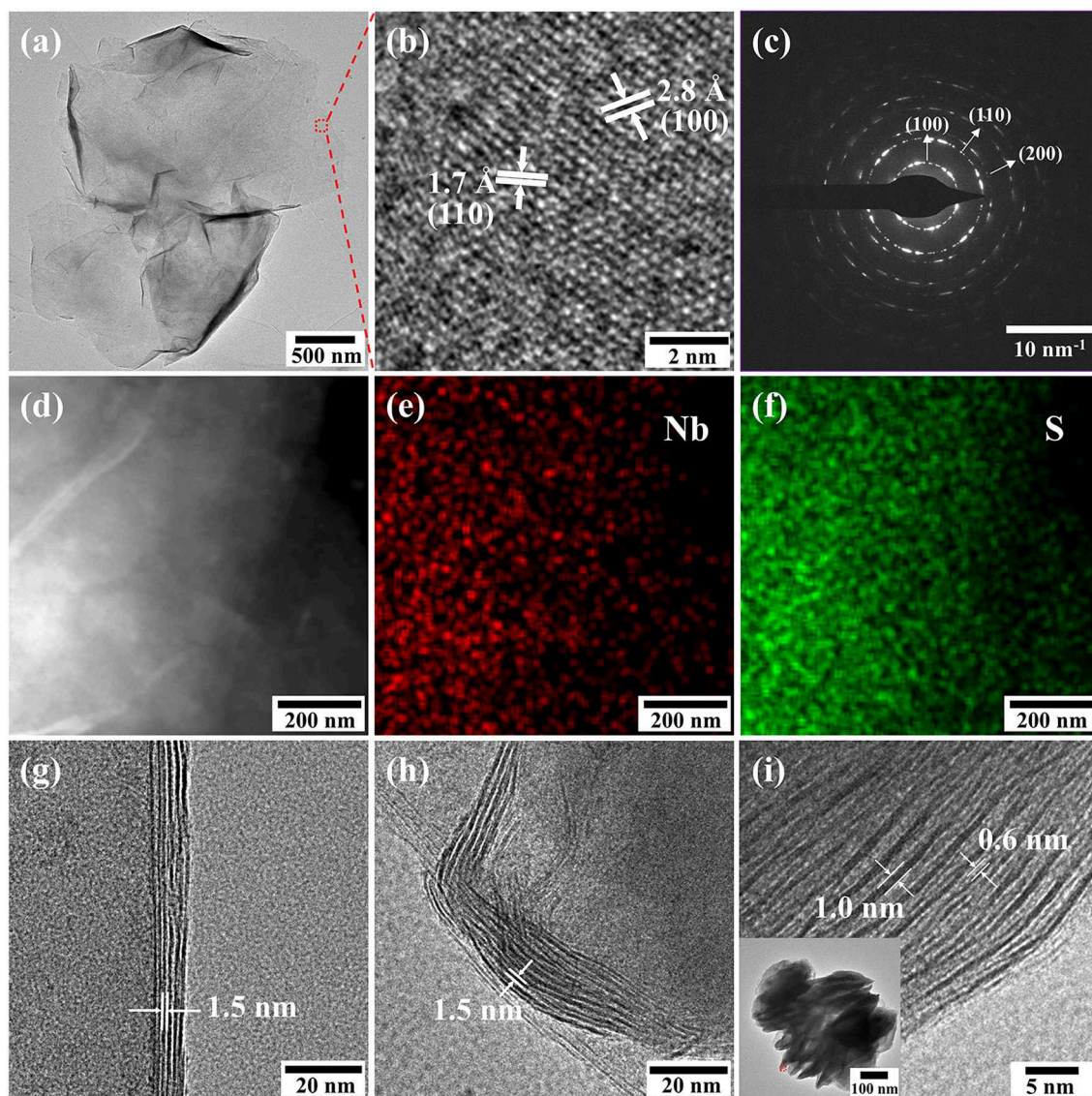


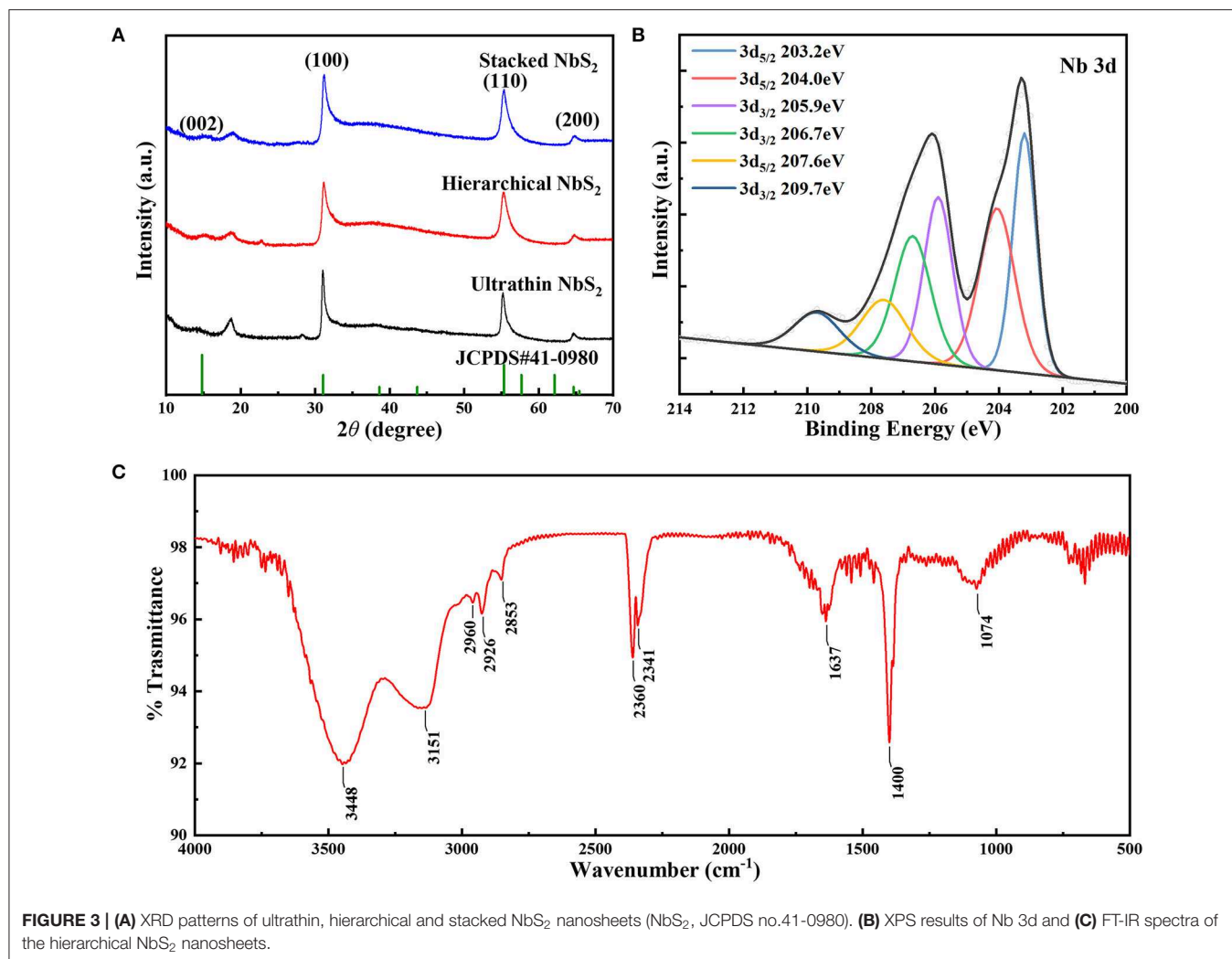
FIGURE 2 | (a) TEM images, (b) HRTEM images and (c) SAED pattern of ultrathin NbS₂ nanosheets. (d–f) Element mapping of ultrathin NbS₂ nanosheets. (g–i) Edges of ultrathin, hierarchical and stacked NbS₂ nanosheets. Inset: TEM images of stacked NbS₂ nanosheets.

layer-to-layer spacings of ultrathin and hierarchical nanosheets were ~ 1.5 nm, indicating the existence of OLA molecules among layers (Jang et al., 2011). The 0.6 nm spacing of stacked nanosheets was consistent with the (002) lattice plane, while the 1.0 nm spacing could also be expanded by OLA molecules. The inset pattern in **Figure 2i** shows the TEM images of stacked NbS₂ nanosheets. The thickness of the NbS₂ nanosheets increased with the amount of CS₂, from 10, 20, to 60 nm.

The crystalline characteristics of the various NbS₂ samples with different morphologies were confirmed by XRD, as shown in **Figure 3A**. The diffraction peaks of all the as-prepared NbS₂ matched with the standard pattern (JCPDS no.41-0980), the peaks at 14.8°, 31.0°, 55.3° and 64.7° could be assigned to (002), (100), (110), and (200) planes of the hexagonal crystal structure

NbS₂ with space group *P63/mmc* (Zhang J. et al., 2017), which was consistent with the lattice fringes of the HRTEM results.

To analyze the surface electronic states of the NbS₂ nanosheets, an XPS survey was carried out. **Figure 3B** shows the Nb 3d spectrum of the hierarchical NbS₂ nanosheets. The binding energies of 3d_{3/2} located at 209.7 eV and 3d_{5/2} at 207.6 eV revealed the existence of Nb⁵⁺ (Zhang J. et al., 2017). The peaks of 3d_{3/2} at 206.7 eV and 3d_{5/2} at 204.0 eV could be assigned to Nb⁴⁺ (Zhang J. et al., 2017). The binding energies of 3d_{3/2} state occurring at 205.9 eV and 3d_{5/2} at 203.2 eV corresponded to the oxidation state of Nb^{(4–δ)+} (Izawa et al., 2008). The Nb 3d and S 2p XPS spectra of ultrathin, hierarchical and stacked NbS₂ nanosheets were summarized in **Figure S2**. In the S 2p



spectrum (Figure S2b), peaks of $2p_{2/3}$ and $2p_{1/2}$ at 160.6 and 161.7 eV respectively, was corresponding to S^{2-} (Dash et al., 2015).

To examine the surfactant on the surface of the samples, an FT-IR test of hierarchical NbS₂ nanosheets ranging from 500 ~ 4,000 cm^{-1} was conducted (Figure 3C). The FT-IR spectra proved the existence of oleylamine (OLA). The two broad absorption peaks at 3448 and 3151 cm^{-1} could be assigned to N-H stretching mode, and peak at 1637 cm^{-1} corresponded to NH₂ scissoring mode (Altavilla et al., 2011; Cooper et al., 2011). The peaks at 2,960 and 2,926 cm^{-1} were due to asymmetrical stretching vibration of CH₃, and the peak at 2,853 cm^{-1} was due to asymmetrical stretching vibration of CH₂ (Altavilla et al., 2011). The broad peak located at 1074 cm^{-1} came from C-N stretching vibration mode (Gunasekaran et al., 2008). The peaks at 2,360 and 2,341 cm^{-1} were attributed to the adsorption doublet band of CO₂. The peak located at 1,400 cm^{-1} could be due to CH₃ symmetric bending vibration (Gunasekaran et al., 2008).

Growth Mechanism of NbS₂ Nanosheets

The shape of nanocrystals is dominated by the surface energy of the facets. For some transition metal dichalcogenides, including NbS₂, 2D shapes are thermodynamically favored (Jeong et al., 2012; Moon, 2018). In the synthesis process of colloidal NbS₂ nanosheets, oleylamine (OLA) serves as an organic surfactant, solvent, and reducing agent, as reported in other colloidal synthesis works (Yin and Alivisatos, 2005). The reaction can be illustrated as the following steps: (1) NbCl₅ and OLA formed complexes by the dissolution of NbCl₅ in OLA (Nasilowski et al., 2016); (2) generation of H₂S gas via the reaction of OLA with CS₂ after the injection of CS₂ (Yoo et al., 2014); (3) reaction of the niobium (V) with H₂S to form Niobium (IV) disulfide monomers; (4) burst of nucleation of NbS₂ crystals; (5) growth of NbS₂ crystals to form nanosheets (Figure 4).

Temperature is an important factor for crystal growth as it can change dynamics of ions and atoms in solution, and also alter the probability of effective collision between atoms. The adhesion of OLA molecules as surfactant to the NbS₂ nanocrystal surfaces can form NbS₂ - OLA complexes, and the stability and

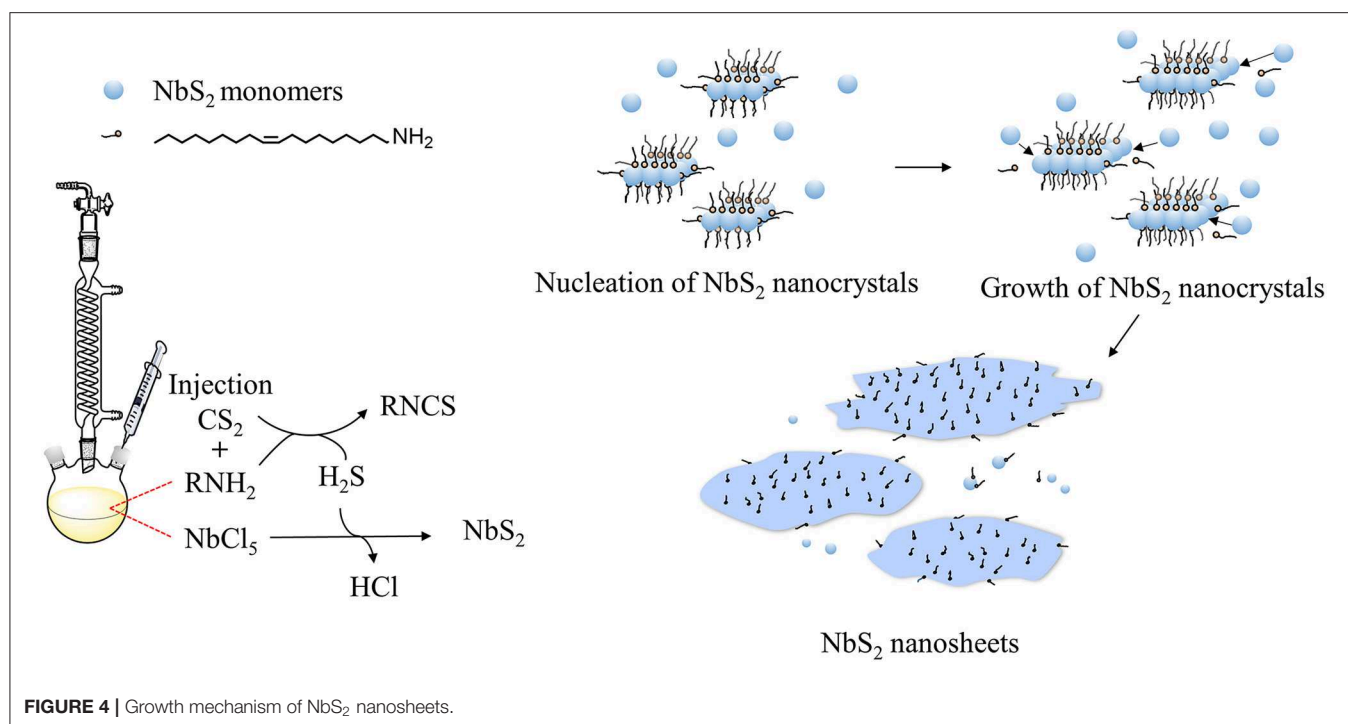


FIGURE 4 | Growth mechanism of NbS₂ nanosheets.

motion rate can be adjusted by the growth temperature. The OLA molecules should be capable of exchanging on and off the surface of growing crystals for instantaneous growth (Yin and Alivisatos, 2005). As the temperature rises, the stability of the complexes reduces, and OLA molecules have a higher probability of leaving the NbS₂ nanocrystals, then monomers are more likely to access and add to the nanocrystal surface—thus the thickness and lateral size of the nanosheets increase, which is consistent with the experiment results.

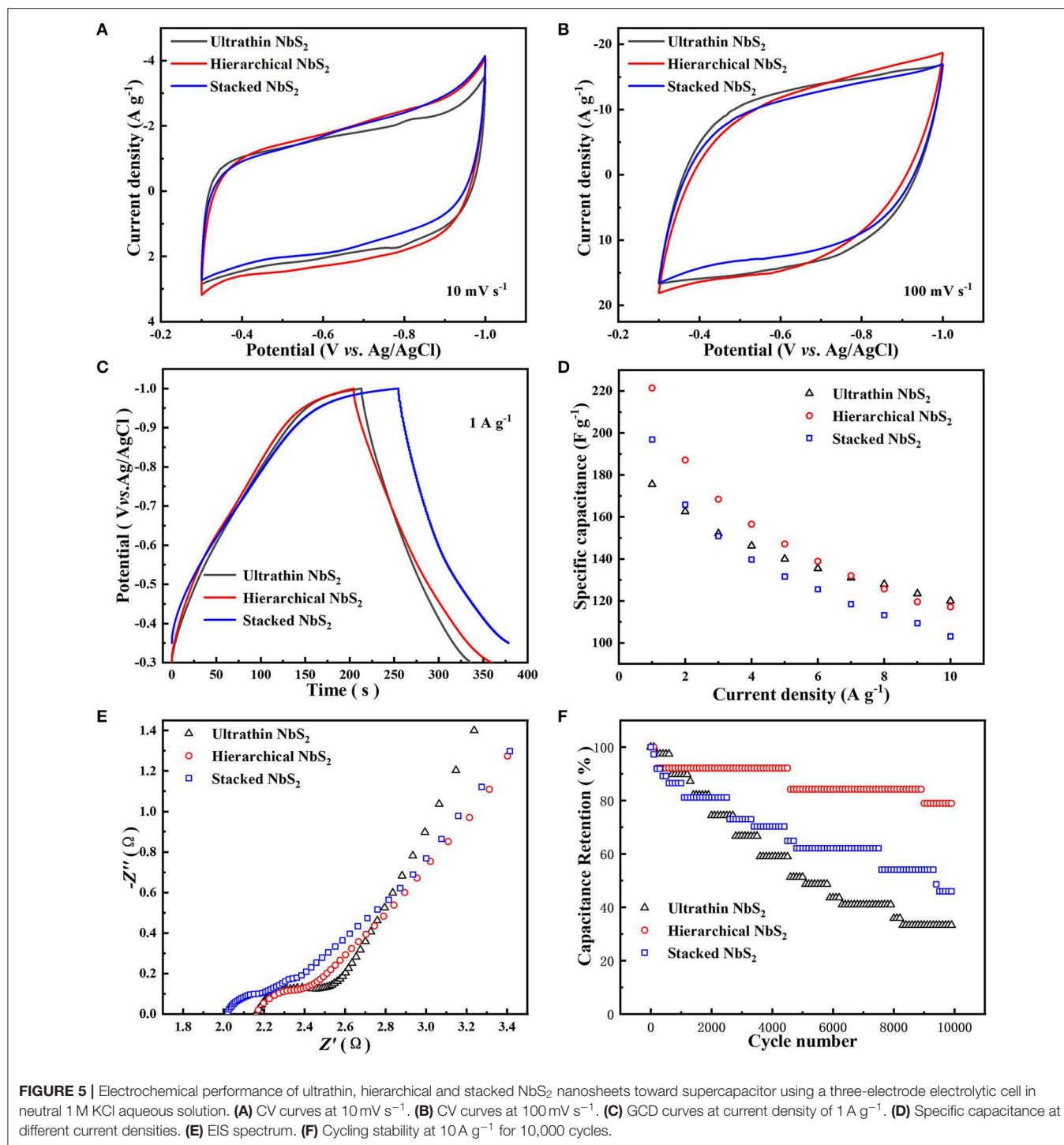
The morphology changes, including lateral size and thickness, caused by the dose of CS₂ can be explained by the following two reasons. On one hand, the amount of CS₂ injected into the reaction system may change the monomer concentration. According to “size-distribution focusing” theory (Yin and Alivisatos, 2005), the critical size of nanocrystals diminishes instantly after injection of precursor for a second time due to the burst of monomers. In the synthesis process of NbS₂ nanocrystals in our experiment, CS₂ was injected slowly (about 0.1 mL/min), so the higher amount of CS₂, the longer the injection time is. Based on the condition that an excess of OLA acts as a reducing agent, and the quick enough reduction of CS₂ by OLA, as well as the rapid reaction between NbCl₅ and H₂S, it is hypothesized that the generation of monomers occur instantly and continuously during the CS₂ injection period, and the critical size of NbS₂ nanocrystals become smaller steadily. On the other hand, owing to crystal surface energy differences and their distinct reactive activity toward sulfur, an increase in the amount of CS₂ promotes vertical growth of anisotropic crystal (Mansouri and Semagina, 2018), and the thickness of nanosheets increases.

The assembly or aggregation of layered nanosheets can be influenced by the surface passivation and polarity of solvent,

owing to the combined effect of solvation and cohesive energy (Zhang X. et al., 2017). The NbS₂ nanosheets tend to assemble or aggregate with the CS₂ amount increase, the possible reason is that more CS₂ or H₂S molecules adsorb to the surface of NbS₂ nanosheets in the reaction solution, and occupy the sites of OLA molecules, thus the surface energy of NbS₂ increases, and an assemble or aggregate phenomenon can more easily to occur.

Electrochemical Performance of NbS₂ Nanosheets

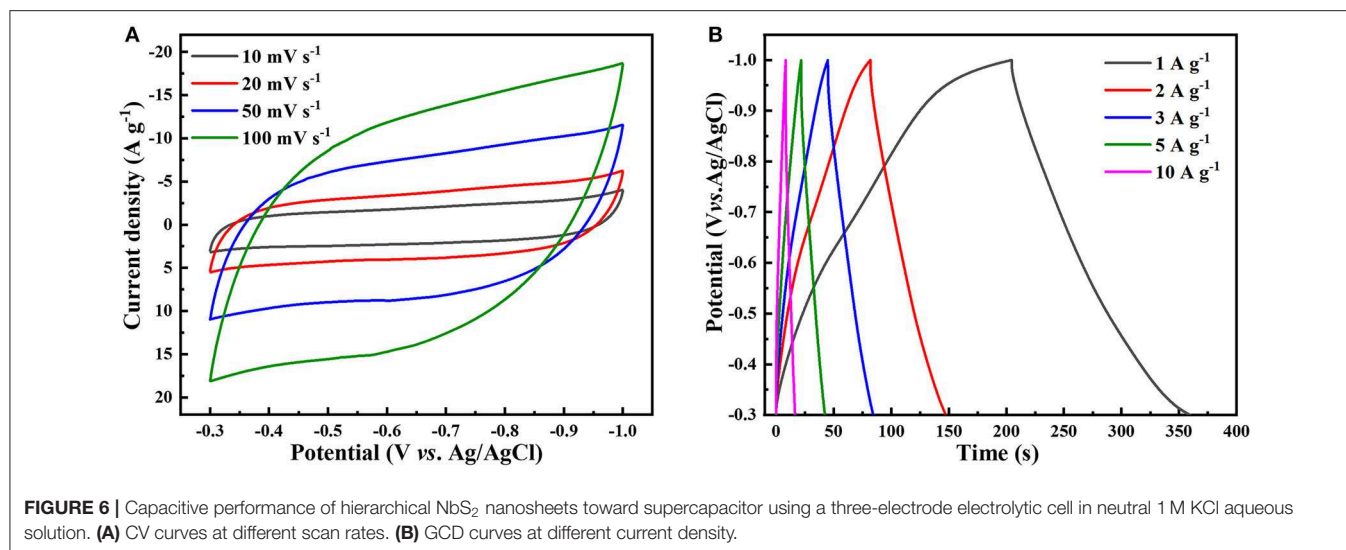
To compare the electrochemical performance differences of NbS₂ nanosheets with diverse morphologies, the electrochemical tests of ultrathin, hierarchical, and stacked NbS₂ nanosheets were investigated as negative electrode materials for a supercapacitor using a three-electrode electrolytic cell in neutral 1 M KCl aqueous solution (Figure 5). The CV curves of three samples all show quasi-rectangular shapes at scan rates of 10 and 100 mV s⁻¹ (Figures 5A,B). There existed weak redox peaks at -0.82 V and -0.78 V (vs. Ag/AgCl) for the ultrathin sample at scan rate of 10 mV s⁻¹, which may be due to faster ion diffusion than the other two samples. The operating voltage windows of galvanostatic charge-discharge (GCD) curves was -0.3 ~ -1 V (vs. Ag/AgCl) for ultrathin and hierarchical NbS₂ electrodes, and -0.35 ~ -1 V (vs. Ag/AgCl) for stacked NbS₂ electrodes because its discharge process was sluggish as the potential came near to -0.3 V (vs. Ag/AgCl) at the current density of 1 A g⁻¹ (Figure 5C). The GCD curves of the ultrathin and hierarchical NbS₂ electrodes performed a good symmetric triangular shape at 1 A g⁻¹, suggesting its rapid and reversible charge-discharge ability (Liu et al., 2018a; Li et al., 2019), while the stacked NbS₂ electrode



showed slow charge process when the potential approached to -1.0 V (vs. Ag/AgCl) (**Figure 5C**). The specific capacitance can be calculated using Equation (S1) or Equation (S2) from **Supplementary Material**. The ultrathin NbS₂ electrode had the highest rate capability, and displayed 120.0 F g⁻¹ at 10 A g⁻¹. However, the hierarchical NbS₂ electrode showed the highest specific capacitance at low current densities (1 to 7 A g⁻¹), displaying 221.4 F g⁻¹ at 1 A g⁻¹ (**Figure 5D**). The

electrochemical energy storage performance of the stacked NbS₂ electrode was poorer than the former two samples at high current densities.

To estimate the ion accessible surface area of NbS₂ nanosheets electrodes, the electrochemical surface area (ECSA) was evaluated using cyclic voltammetry measurement (**Figure S3**). The electrochemical double layer capacitance (C_{EDL}) of the ultrathin, hierarchical, and stacked NbS₂ electrodes were 206.6,



195.8, and 165.5 mF respectively. The C_{EDL} of the ultrathin NbS₂ electrode was the highest among three samples, while its specific capacitance was the lowest in low current densities (1 and 2 A g⁻¹), demonstrating the ECSA was not the only affected factor for the performance of specific capacitance. The ECSA may play a more important role in the rapid charge and discharge process as the specific capacitance of ultrathin NbS₂ electrodes was the highest in high current densities (8, 9, and 10 A g⁻¹).

The EIS test was carried out to understand the internal resistance of the various NbS₂ electrodes and interactions of the electrode/electrolyte interface. As shown in **Figure 5E**, the Nyquist plots displayed semicircles in the high frequency region, relating to charge transfer resistance (R_{ct}) (Liu et al., 2018b). The R_{ct} value of the hierarchical NbS₂ electrode was smaller than the ultrathin one, reflecting the easier process of charge transfer, which was coherent with the results that the specific capacitance of the former electrode was higher than the latter one in low current densities (**Figure 5D**). The slope of the ultrathin NbS₂ electrode was the steepest among the three samples in the low frequency region, indicating more efficient ion diffusion, which was consistent with the higher rate capability shown in **Figure 5D**.

To test the potential application of NbS₂ in practical uses, the cycling stability test was carried out at current density of 10 A g⁻¹. The hierarchical NbS₂ electrode exhibited capacitance retention with 78.9% of the initial specific capacitance after 10 000 cycles—much better than the ultrathin and stacked NbS₂ electrodes (**Figure 5F**). The structure of the hierarchical NbS₂ sample maintained well after the stability test, indicating that decay of capacitance may mainly be due to the exfoliation of partial active materials from the electrode (**Figure S4**). However, both the ultrathin and stacked NbS₂ nanosheets aggregated to some extent, consistent with poor stability.

As the hierarchical NbS₂ electrode showed better overall electrochemical performance than the ultrathin or stacked NbS₂ electrode, and the capacitive characteristics of the three electrodes are similar, we only discuss the capacitive performance

of the hierarchical NbS₂ electrode in more detail here. The capacitive performance of ultrathin and stacked NbS₂ electrodes can be obtained from supporting information (**Figure S6**). **Figure 6A** shows the CV curves of the hierarchical NbS₂ electrode tested at scan rates from 10 to 100 mV s⁻¹ in the potential range of -0.3 ~ -1 V (vs. Ag/AgCl), which displayed quasi-rectangular shapes, indicating the electrochemical double layer capacitance (EDLC) mechanism primarily (Peng et al., 2019). The hierarchical NbS₂ electrode material occasioned oxidation reaction when the operating voltage window was broadened to -0.2 ~ -1 V and -0.1 ~ -1 V (vs. Ag/AgCl), as the CV curves at 50 mV s⁻¹ shows (**Figure S5**).

The GCD curves of NbS₂ electrodes indicated the capacitive behavior at different current densities. The near-triangular GCD curves of the hierarchical NbS₂ recorded from 1 to 10 A g⁻¹ are shown in **Figure 6B**, exhibiting good specific capacitance of 221.4 F g⁻¹ at 1 A g⁻¹ and 117.1 F g⁻¹ at 10 A g⁻¹, respectively. The CV curves and the GCD curves of the ultrathin and stacked NbS₂ are presented in **Figure S6**. The specific capacitance of ultrathin NbS₂ was 175.6 F g⁻¹ at 1 A g⁻¹ and 120.0 F g⁻¹ at 10 A g⁻¹, respectively. And the specific capacitance of stacked NbS₂ was 196.9 F g⁻¹ at 1 A g⁻¹ and 103.1 F g⁻¹ at 10 A g⁻¹, respectively.

From the electrochemical analysis, the hierarchical NbS₂ electrode showed great overall electrochemical performance for energy storage. Fast and efficient electron transfer of the electrode can be achieved owing to the small charge transfer resistance. Furthermore, the restacking or aggregation of nanosheets can be suppressed by constructing a hierarchical structure, and the electrochemical active materials can be fully utilized during long-term charging and discharging processes.

CONCLUSIONS

In summary, we introduce a colloidal synthesis method to regulate the morphologies of colloidal NbS₂ nanocrystals via dynamics control. The size, thickness, and structure

of nanocrystals can be adjusted by controlling the growth temperature and CS₂ amount. The ultrathin NbS₂ nanosheets show more efficient ion diffusion in the application of supercapacitor, while the self-assembled hierarchical structure NbS₂ can suppress the restacking or aggregation of nanosheets effectively. This work offers insight into morphology regulation of layered TMDs in the synthesis process. The self-assembling mechanism has not yet been fully understood and needs to be investigated in future research.

DATA AVAILABILITY STATEMENT

All datasets generated for this study are included in the article/**Supplementary Material**.

AUTHOR CONTRIBUTIONS

WL (Investigation: Lead, Methodology: Lead, Writing – original draft: Lead, Writing – review and editing: Lead).

REFERENCES

- Altavilla, C., Sarno, M., and Ciambelli, P. (2011). A novel wet chemistry approach for the synthesis of hybrid 2D free-floating single or multilayer nanosheets of MS₂@oleylamine (M=Mo, W). *Chem. Mater.* 23, 3879–3885. doi: 10.1021/cm200837g
- Cha, J.-H., Choi, S.-J., Yu, S., and Kim, I.-D. (2017). 2D WS₂-edge functionalized multi-channel carbon nanofibers: effect of WS₂ edge-abundant structure on room temperature NO₂ sensing. *J. Mater. Chem. A* 5, 8725–8732. doi: 10.1039/C6TA11019C
- Chen, W., Gui, X., Yang, L., Zhu, H., and Tang, Z. (2019). Wrinkling of two-dimensional materials: methods, properties and applications. *Nanoscale Horiz.* 4, 291–320. doi: 10.1039/C8NH00112J
- Chhowalla, M., Shin, H. S., Eda, G., Li, L. J., Loh, K. P., and Zhang, H. (2013). The chemistry of two-dimensional layered transition metal dichalcogenide nanosheets. *Nat. Chem.* 5, 263–275. doi: 10.1038/nchem.1589
- Cho, K., Pak, J., Chung, S., and Lee, T. (2019). Recent advances in interface engineering of transition-metal dichalcogenides with organic molecules and polymers. *ACS Nano* 13, 9713–9734. doi: 10.1021/acsnano.9b02540
- Cong, L., Xie, H., and Li, J. (2017). Hierarchical structures based on two-dimensional nanomaterials for rechargeable lithium batteries. *Adv. Energy Mater.* 7:1601906. doi: 10.1002/aenm.201601906
- Cooper, J. K., Franco, A. M., Gul, S., Corrado, C., and Zhang, J. Z. (2011). Characterization of primary amine capped CdSe, ZnSe, and ZnS Quantum dots by FT-IR: determination of surface bonding interaction and identification of selective desorption. *Langmuir* 27, 8486–8493. doi: 10.1021/la201273x
- Dash, J. K., Chen, L., Dinolfo, P. H., Lu, T.-M., and Wang, G.-C. (2015). A method toward fabricating semiconducting 3R-NbS₂ ultrathin films. *J. Phys. Chem. C* 119, 19763–19771. doi: 10.1021/acs.jpcc.5b04057
- Gunasekaran, S., Natarajan, R. K., Renganayaki, V., and Rathikha, R. (2008). FTIR and UV visible spectrophotometric approach to discriminate leukemic sera. *Asian J. Chem.* 20, 2521–2530.
- Han, J. H., Kim, H. K., Baek, B., Han, J., Ahn, H. S., Baik, M., et al. (2018). Activation of the basal plane in two dimensional transition metal chalcogenide nanostructures. *J. Am. Chem. Soc.* 140, 13663–13671. doi: 10.1021/jacs.8b05477
- Izawa, K., Ida, S., Unal, U., Yamaguchi, T. J., Kang, H. J., Choy, H., et al. (2008). A new approach for the synthesis of layered niobium sulfide and restacking route of NbS₂ nanosheet. *J. Solid State Chem.* 181, 319–324. doi: 10.1016/j.jssc.2007.12.002
- Jang, J. T., Jeong, S., Seo, J. W., Kim, M. C., Sim, E., Oh, Y., et al. (2011). Ultrathin zirconium disulfide nanodiscs. *J. Am. Chem. Soc.* 133, 7636–7639. doi: 10.1021/ja200400n
- XW (Investigation: Supporting, Writing – review and editing: Supporting). HD and YO (Writing – review and editing: Supporting). SX and YY (Software: Supporting). PX and YZ (Supervision: Lead, Writing – review and editing: Lead).

FUNDING

This work was supported by the Project of State Key Laboratory of Environment Friendly Energy Materials, the Southwest University of Science and Technology (No. 17FKSY0115).

SUPPLEMENTARY MATERIAL

The Supplementary Material for this article can be found online at: <https://www.frontiersin.org/articles/10.3389/fchem.2020.00189/full#supplementary-material>

Jeong, S., Yoo, D., Jang, J. T., Kim, M., and Cheon, J. (2012). Well-defined colloidal 2-D layered transition-metal chalcogenide nanocrystals via generalized synthetic protocols. *J. Am. Chem. Soc.* 134, 18233–18236. doi: 10.1021/ja3089845

Kuc, A. B., Zibouche, N., and Heine, T. (2011). Influence of quantum confinement on the electronic structure of the transition metal sulfide TS₂. *Phys. Rev. B* 83:245213. doi: 10.1103/PhysRevB.83.245213

Li, Y., Tang, X., Zhou, X., Li, L., and Jiang, S. (2019). Improvement of lithium ion storage in titanium dioxide nanowires by introducing interfacial capacity. *Appl. Surf. Sci.* doi: 10.1016/j.apsusc.2019.144649. [Epub ahead of print].

Li, Y., Wang, H., Xie, L., Liang, Y., Hong, G., and Dai, H. (2011). MoS₂ nanoparticles grown on graphene: an advanced catalyst for the hydrogen evolution reaction. *J. Am. Chem. Soc.* 133, 7296–7299. doi: 10.1021/ja201269b

Lin, L., Lei, W., Zhang, S., Liu, Y., Wallace, G. G., and Chen, J. (2019). Two-dimensional transition metal dichalcogenides in supercapacitors and secondary batteries. *Energy Storage Mater.* 19, 408–423. doi: 10.1016/j.ensm.2019.02.023

Lin, Y. C., Jariwala, B., Bersch, B. M., Xu, K., Nie, Y., Wang, B., et al. (2018). Realizing large-scale, electronic-grade two-dimensional semiconductors. *ACS Nano* 12, 965–975. doi: 10.1021/acsnano.7b07059

Linhart, L., Paur, M., Smejkal, V., Burgdörfer, J., Mueller, T., and Libisch, F. (2019). Localized intervalley defect excitons as single-photon emitters in WSe₂. *Phys. Rev. Lett.* 123:146401. doi: 10.1103/PhysRevLett.123.146401

Liu, X., Sheng, G., Zhong, M., and Zhou, X. (2018a). Dispersed and size-selected WO₃ nanoparticles in carbon aerogel for supercapacitor applications. *Mater. Des.* 141, 220–229. doi: 10.1016/j.matdes.2017.12.038

Liu, X., Sheng, G., Zhong, M., and Zhou, X. (2018b). Hybrid nanowires and nanoparticles of WO₃ in a carbon aerogel for supercapacitor applications. *Nanoscale* 10, 4209–4217. doi: 10.1039/C7NR07191D

Mak, K. F., and Shan, J. (2016). Photonics and optoelectronics of 2D semiconductor transition metal dichalcogenides. *Nat. Photonics* 10, 216–226. doi: 10.1038/nphoton.2015.282

Mansouri, A., and Semagina, N. (2018). Colloidal synthesis protocol of shape- and dimensionally-controlled transition-metal chalcogenides and their hydrodesulfurization activities. *ACS Appl. Nano Mater.* 1, 4408–4412. doi: 10.1021/acsnm.8b01353

Mei, J., Zhang, Y., Liao, T., Sun, Z., and Dou, S. X. (2018). Strategies for improving the lithium-storage performance of 2D nanomaterials. *Natl. Sci. Rev.* 5, 389–416. doi: 10.1093/nsr/nwx077

Moon, G. D. (2018). *Anisotropic Metal Chalcogenide Nanomaterials: Synthesis, Assembly, and Applications*. Busan: Springer. doi: 10.1007/978-3-030-03943-1

- Muller, G. A., Cook, J. B., Kim, H. S., Tolbert, S. H., and Dunn, B. (2015). High performance pseudocapacitor based on 2D layered metal chalcogenide nanocrystals. *Nano Lett.* 15, 1911–1917. doi: 10.1021/nl504764m
- Nasilowski, M., Mahler, B., Lhuillier, E., Ithurria, S., and Dubertret, B. (2016). Two-dimensional colloidal nanocrystals. *Chem. Rev.* 116, 10934–10982. doi: 10.1021/acs.chemrev.6b00164
- Peng, H., Yao, B., Wei, X., Liu, T., Kou, T., Xiao, P., et al. (2019). Pore and heteroatom engineered carbon foams for supercapacitors. *Adv. Energy Mater.* 9:1803665. doi: 10.1002/aenm.201803665
- Sun, P., Zhang, W., Hu, X., Yuan, L., and Huang, Y. (2014). Synthesis of hierarchical MoS₂ and its electrochemical performance as an anode material for lithium-ion batteries. *J. Mater. Chem. A* 2, 3498–3504. doi: 10.1039/C3TA13994H
- Wang, C., Wu, X., Xu, H., Zhu, Y., Liang, F., Luo, C., et al. (2019). VSe₂/carbon-nanotube compound for all solid-state flexible inplane supercapacitor. *Appl. Phys. Lett.* 114. doi: 10.1063/1.5078555
- Wang, Q. H., Kalantar-Zadeh, K., Kis, A., Coleman, J. N., and Strano, M. S. (2012). Electronics and optoelectronics of two-dimensional transition metal dichalcogenides. *Nat. Nanotechnol.* 7, 699–712. doi: 10.1038/nnano.2012.193
- Yan, Y., Xia, B., Xu, Z., and Wang, X. (2014). Recent development of molybdenum sulfides as advanced electrocatalysts for hydrogen evolution reaction. *ACS Catal.* 4, 1693–1705. doi: 10.1021/cs500070x
- Yang, J., Mohmad, A. R., Wang, Y., Fullon, R., Song, X., Zhao, F., et al. (2019). Ultrahigh-current-density Niobium disulfide catalysts for hydrogen evolution. *Nat. Mater.* 18, 1309–1314. doi: 10.1038/s41563-019-0463-8
- Yang, P., Zhang, Z., Shi, J., Jiang, S., and Zhang, Y. (2017). Progress in controllable construction and energy-related applications of MX₂/Graphene and MX₂/MX₂ heterostructures. *ChemNanoMat* 3, 340–351. doi: 10.1002/cnma.201700031
- Yin, Y., and Alivisatos, A. P. (2005). Colloidal nanocrystal synthesis and the organic-inorganic interface. *Nature* 437, 664–670. doi: 10.1038/nature04165
- Yoo, D., Kim, M., Jeong, S., Han, J., and Cheon, J. (2014). Chemical synthetic strategy for single-layer transition-metal chalcogenides. *J. Am. Chem. Soc.* 136, 14670–14673. doi: 10.1021/ja5079943
- Yun, Q., Li, L., Hu, Z., Lu, Q., Chen, B., and Zhang, H. (2020). Layered transition metal dichalcogenide-based nanomaterials for electrochemical energy storage. *Adv. Mater.* 32:e1903826. doi: 10.1002/adma.201903826
- Zhang, J., Du, C., Dai, Z., Chen, W., Zheng, Y., Li, B., et al. (2017). NbS₂ nanosheets with M/Se (M = Fe, Co, Ni) Codopants for Li⁺ and Na⁺ Storage. *ACS Nano* 11, 10599–10607. doi: 10.1021/acsnano.7b06133
- Zhang, X., Cheng, H., and Zhang, H. (2017). Recent progress in the preparation, assembly, transformation, and applications of layer-structured nanodisks beyond graphene. *Adv. Mater.* 29:1701704. doi: 10.1002/adma.201701704

Conflict of Interest: The authors declare that the research was conducted in the absence of any commercial or financial relationships that could be construed as a potential conflict of interest.

Copyright © 2020 Li, Wei, Dong, Ou, Xiao, Yang, Xiao and Zhang. This is an open-access article distributed under the terms of the Creative Commons Attribution License (CC BY). The use, distribution or reproduction in other forums is permitted, provided the original author(s) and the copyright owner(s) are credited and that the original publication in this journal is cited, in accordance with accepted academic practice. No use, distribution or reproduction is permitted which does not comply with these terms.